Marine Pollution Bulletin 168 (2021) 112440

Contents lists available at ScienceDirect

Marine Pollution Bulletin

journal homepage: www.elsevier.com/locate/marpolbul

Microbial nitrogen loss by coupled nitrification to denitrification and anammox in a permeable subterranean estuary at Gloucester Point, Virginia

Jiapeng Wu [a], Yiguo Hong [a,b,*], Stephanie J. Wilson [c], Bongkeun Song [c,**]

[a] Institute of Environmental Research at Greater Bay Area, Key Laboratory for Water Quality and Conservation of the Pearl River Delta, Ministry of Education, Guangzhou University, Guangzhou 510006, China
[b] School of Environmental Science and Engineering, Guangzhou University, Guangzhou 510006, China
[c] Department of Biological Sciences, Virginia Institute of Marine Science, College of William & Mary, Gloucester Point, USA

ARTICLE INFO

Keywords:
Subterranean estuary
Aerobic-anaerobic transition zone
Nitrogen loss hotspots
Community composition

ABSTRACT

The nitrogen (N) loss processes have not been well examined in subterranean estuaries (STEs) between land and sea. We utilized a ^{15}N isotope tracer method, q-PCR, and high-throughput sequencing to reveal the activities, abundances, and community compositions of N loss communities in a STE in Gloucester Point, Virginia, US. The highest activities, abundances and diversity of denitrifiers and anammox bacteria were detected at 50–60 cm depth in the aerobic-anaerobic transition zone (AATZ) characterized by sharp redox gradients. *nirS*-denitrifiers and anammox bacteria were affiliated to 10 different clusters and three genera, respectively. Denitrification and anammox played equal roles with an estimated N loss of 13.15 mmol N m^{-3} day^{-1}. A positive correlation between ammonia oxidizing prokaryote abundances and DO as well as NO_x^- suggested that nitrification produces NO_x^- which supports the hotspot of denitrification and anammox within the AATZ. Overall, these results highlight the roles of N loss communities in STEs.

1. Introduction

Land-sea transition zones play an important role in buffering the open ocean from anthropogenic nitrogen (N) inputs by acting as highly efficient bioreactors. Roughly >70% of ice-free continental shelves are covered by sandy beaches (Luijendijk et al., 2018). Freshwater and seawater exchange at the coastline occurs in highly permeable beaches or subterranean estuaries (STEs) with steep redox, salinity and oxygen gradients. Ahrens et al. (2020) found that STEs with permeable sandy sediment are complex environments and highly active, supporting many biogeochemical reactions, such as desorption of ions (Charette and Sholkovitz, 2002), dissolution and precipitation of carbonates (Liu et al., 2017), remineralization of organic matter (Roy et al., 2013), metal release (O'Connor et al., 2018) and nutrient transformations (Couturier et al., 2017; Jiao et al., 2018; Santos et al., 2008).

Rivers and estuaries have long been regarded as major areas of N removal prior to the ocean (Seitzinger et al., 2005). Voss et al. (2013) found that N loads from submarine groundwater discharge (SGD, 4 Tg N yr^{-1}) were unexpectedly higher than previously realized. Cho et al. (2018) reported that total SGD-derived flues of DIN could be 1.4-fold higher than river fluxes to the global ocean. SGD plays a major role in N cycling in coastal and marine environmental water quality (Beusen et al., 2013; Couturier et al., 2017). Microbial communities and their functions in the STE along the subsurface freshwater–seawater continuum determine the fate of N discharged to coastal waters (Santoro, 2010). Assessing the role of microbial N loss processes in the STE is crucial to understanding coastal ecosystems as a buffer from anthropogenic N inputs and reducing the development of harmful algal blooms in coastal waters.

Denitrification and anaerobic ammonium oxidation (anammox) are two major processes removing excess N from coastal ecosystems (Hong et al., 2019a; Ward, 2013). Due to large variation typically found in STEs, which are highly heterogeneous systems, microbial N loss processes are also highly variable. Fluctuating hydrological regimes with intense material exchange at the interface between two adjacent ecosystems creates the potential for biogeochemical hotspots (Zhu et al., 2013). Under similar dynamic hydrologic conditions, the aerobic-anaerobic transition zone (AATZ) in STEs is regarded as hotspot of

* Correspondence to: Y. Hong, Institute of Environmental Research at Greater Bay Area, Key Laboratory for Water Quality and Conservation of the Pearl River Delta, Ministry of Education, Guangzhou University, Guangzhou 510006, China.
** Corresponding author.
E-mail addresses: yghong@gzhu.edu.cn (Y. Hong), songb@vims.edu (B. Song).

https://doi.org/10.1016/j.marpolbul.2021.112440
Received 8 January 2021; Received in revised form 29 March 2021; Accepted 26 April 2021
Available online 8 May 2021

biogeochemical processes with the highest diversity and abundance of microorganisms and complex predicted microbial functions (Hong et al., 2019b). Nevertheless, our knowledge about the microbial N loss processes in the AATZ of STEs remains under-studied.

Previously, denitrification capacity and microbial N attenuation in the STEs have been evaluated by in situ injections of ^{15}N-nitrate (push-pull method) (Addy et al., 2005) and the reduction of DIN inventory during transit (Gonneea and Charette, 2014). Microbial N loss occurred in the deeper, suboxic regions of the STE, whereas in surficial sediment, NO_3^- did not encounter favorable condition for N loss (Santoro, 2010). Smith et al. (2015) found active anammox in all areas tested in a coastal aquifer by quantifying changes in $^{28,29,30}N_2$, $^{15}NO_X^-$ and $^{15}NH_4^+$ with groundwater travel time. Ladderane fatty acid analysis also showed that anammox bacteria were prevalent in the upper portion of a STE (Sáenz et al., 2012). N loss processes are largely controlled by residence time length (Gonneea and Charette, 2014), redox state dynamics (Slomp and Van Cappellen, 2004), and substrate availability (Sáenz et al., 2012) in the STE. Until now, the microbial communities of N loss processes and their distribution pattern in permeable STEs are unclear.

Employing molecular detection techniques is a straightforward way to understand what types of microorganisms exist in STEs (Santoro, 2010). The polymerase chain reaction (PCR), performed with specific primers of N cycling genes (e.g., *amoA*, *nirS*, and *nosZ*I/II), combined with sequencing techniques (e.g., clone library and high through-put sequencing) can determine the community composition and diversity of N-cycling microorganisms. In addition, quantitative PCR was developed to assess their abundance. Zheng et al. (2016a) used PCR-based clone library and terminal restriction fragment length polymorphism (T-RFLP) analyses to analyze the denitrification and anammox bacteria in intertidal sediment cores. Jiao et al. (2018) reported high diversity and complex community composition of denitrification and anammox bacteria in STEs with low permeability using high-throughput sequencing. In addition, Hong et al. (2019b) found vertical stratification of microbial communities in the GP-STE by high-throughput sequencing of 16S rRNA gene. Little is known about how the microbial communities mediate N loss processes in permeable STEs, which cope with significant vertical fluctuations in oxygen, dissolved inorganic nitrogen (DIN) availability and other geochemical properties.

Based on these previous studies, we hypothesize that the AATZ is a hotspot of N loss mediated by denitrifying and anammox communities in STE. The redox gradients and availability of NO_x^- and NH_4^+ promote the coupling of nitrification and denitrification and anammox to remove fixed N in the AATZ of GP-STE. Thus, the objectives of this study are (1) to investigate the activity, abundance, and community composition of denitrifying and anammox communities in the sediment along a depth profile of GP-STE, and (2) to identify the location of N loss hotspots in the STE. This study was intended to achieve a more comprehensive understanding of microbial N loss communities and their role in the subsurface N cycle of the GP-STE.

2. Material and methods

2.1. Study area, sampling, and assay of physicochemical parameters

The permeable STE used in this study is located at Gloucester Point (37.248884 N, 76.505324 W), VA, within the Chesapeake Bay. The site description, sampling details and analytical methodology were previously reported by Beck et al. (2016) and Hong et al. (2019b). In brief, one sediment core (90 cm in length), comprised of fine to coarse sands, was sampled at the low tide line at low tide on 15 October of 2015. The SGD rates in GP-STE ranged from 3.9 to 8.9 cm day^{-1}. The York River is microtidal, with a range of ~0.8 m at the study site. The salinity in surface water at the site ranges between 15 and 25 psu (Beck et al., 2016). Sediment core was artificially separated at 10 cm intervals, from GP1 to 10. Groundwater was sampled to correspond to core sample depths (Hong et al., 2019b). Groundwater properties including salinity, dissolved oxygen (DO), oxidation-reduction potential (ORP), temperature, pH, iron (Fe) and dissolved N_2O concentrations, were previously reported in Hong et al. (2019b). Rapid and high-throughput microplate spectrophotometric methods with microplate reader (Tecan Sunrise, Switzerland), described by Wu et al. (2016) and Guan et al. (2017), were used for the determinations of NO_x^- and NH_4^+ contents, respectively. The lowest detection limits for NO_x^- and NH_4^+ were 0.5 and 0.4 μM, respectively.

2.2. Potential activity measurements

The potential rates and contribution to N_2 production of denitrification and anammox in the GP-STE sediments were measured and calculated using a modified method of Dalsgaard and Thamdrup (2002) and Song and Tobias (2011). The incubation condition and measuring instrument of $^{29}N_2$ and $^{30}N_2$ concentration were modified in this study. In brief, 2 g of sediment was transferred to 12.5 mL Exetainer tubes (Labco, High Wycombe, United Kingdom), which were sealed with septa and flushed with He gas. The tubes with sediments were incubated overnight at room temperature to reduce the background levels of NO_x^- and O_2. After pre-incubation, the tubes were divided into three groups, which were spiked through the septum with helium-purged stock solutions of (1) $^{15}NH_4^+$ (^{15}N at 99.6%), (2) $^{15}NH_4^+ + {}^{14}NO_2^-$ and (3) $^{14}NH_4^+ + {}^{15}NO_3^-$ (^{15}N at 99%), respectively. The final concentrations of ^{15}N in all the tubes were approximately 100 μmol L^{-1}. Time course incubations were carried out in duplicate (time points 0, 4, and 8 h) at room temperature. The incubation was stopped by injecting 200 μL of 50% $ZnCl_2$ solution at each time point. The concentrations of $^{29}N_2$ and $^{30}N_2$ produced over the incubation period were measured by a continuous-flow isotope ratio mass spectrometer (Thermo Delta V Advantage, Thermo Scientific) in line with an automated gas bench interface (Thermo Gas Bench II).

2.3. DNA extraction and qPCR assay of N cycling genes

The procedure of DNA extraction was previously reported by Hong et al. (2019b). qPCR assays of the *amoA*, *nirS*, *nosZ*I, *nosZ*II, and anammox specific-16S rRNA genes were performed to quantify the abundance of ammonia oxidizing prokaryotes, denitrifying and anammox bacteria in the sediments, respectively. The qPCR reactions were performed in triplicate with the following primer sets amoA-1F/amoA-2R (Rotthauwe et al., 1997), Arch-amoAF/Arch-amoAR (Francis et al., 2005), cd3aF/R3cd (Throbäck et al., 2004), nosZ1f/nosZ1r, nosZIIF/nosZIIR (Jones et al., 2013) and A438f/A684r (Wu et al., 2019a) using ABI Prism 7500 Real Time PCR System (Applied Biosystems, Carlsbad, CA). Further details concerning primers and PCR conditions can be found in Table S1.

2.4. PCR amplification and sequencing

PCR was conducted to amplify the *nirS* gene of denitrification and the anammox specific-16S rRNA gene using cd3aF/R3cd and A438f/A684r primers, respectively. The forward primer of cd3aF and A438f were attached to a unique 8 bp barcode sequence. The purified PCR products were quantified and sequenced on the Illumina MiSeq platform, generating 250 bp paired-end reads. More details concerning the primers, PCR conditions and sequencing methods can be found in Table S1. Bioinformatic analysis of sequences was conducted using Mothur software v.1.39.1 following the protocol described previously (Jiao et al., 2018; Wu et al., 2019a,b). The raw reads of *nirS* and anammox 16S rRNA gene sequences were deposited in the NCBI short-read archive under the accession numbers PRJNA530374 and PRJNA530365, respectively.

2.5. Statistical analysis

The relationship among the activities, abundances of microbial N loss community (including ammonia oxidizing bacteria (AOB),

ammonia oxidizing archaea (AOA), denitrifiers and anammox bacteria), and sediment characteristics were examined by Pearson correlation analysis using R (version 3.3.3) (Table S2). Redundancy analysis (RDA) was performed using Canoco 5.0 software. Matlab (version R2016a), and Sigmaplot (12.5) software were used for graphics.

3. Results

3.1. Vertical variations of physicochemical parameters

Depth profiles of physicochemical parameters, including salinity, DO, ORP, temperature, pH, Fe(II), Fe(III), Fe(total), and N_2O concentrations were described in detail previously (Hong et al., 2019b). The DO sharply declined from 7.3 ppm at 30 cm to 0.14 ppm at a depth of 90 cm (Fig. 1a, blue dots). In line with the distribution pattern of DO, the salinity declined from 17.80 psu at 30 cm to 1.26 psu at a depth of 90 cm (Fig. 1a, light blue dots). The NH_4^+ profile revealed a sharp increase from 4.47 μM at 30 cm to 60.33 μM at a depth of 90 cm (Fig. 1a, light green triangles). The NO_x^- increased slightly from 30.21 μM at 30 cm to 35.35 μM at 40 cm, and then declined sharply to below the detection limit at 80 cm (Fig. 1a, purple triangles).

3.2. Depth profiles of microbial abundances

The abundances of AOB and AOA showed a surficial depth maximum (Fig. 1b, yellow and blue bars). The abundance of AOB ranged from 0.03 to 1.62×10^2 copies g^{-1}, while AOA abundance ranged from 0 to 4.27×10^2 copies g^{-1} and decreased with sediment depth. The ratio of AOA/AOB abundance in GP1-GP6 ranged from 1.13 to 3.34 (Fig. 1d, pink dots), suggesting AOA was the dominant ammonia oxidizing microbial group. AOB dominate the ammonia oxidizing community in GP8–10. Hong et al. (2019b) previously revealed that microbial abundances, including bacteria and archaea, in the same sediment core ranged from $(0.23 \pm 0.03) \times 10^9$ to $(4.62 \pm 0.08) \times 10^9$ copies g^{-1} dry sediment. The peak microbial abundance in sediment core was observed in GP7.

The abundance of *nirS* and *nosZ*I genes of denitrifiers varied insignificantly with sediment depth ($p > 0.05$, GP1–6), but highest values were observed at GP7 within the AATZ (Fig. 1c and e, green and blue bars). The abundance of *nirS* gene ranged from 0.03 to 8.19×10^5 copies g^{-1} (Fig. 1c, green bars), while *nosZ*I abundance ranged from 0.99 to 5.36×10^5 copies g^{-1} (Fig. 1e, blue bars). The abundances of *nosZ*II gene (Fig. 1e, dark pink bars) were two orders of magnitude higher than *nirS* and *nosZ*I genes (ranged from 0.11 to 4.86×10^7 copies g^{-1}), suggesting *nosZ*II N_2O-reducers were the dominant N_2O sink in STE. Along the sediment depth, the highest value was observed at GP8. Abundances of *nirS*, *nosZ*I and II in bottom sediments (GP9–10) were significantly lower than other layers ($p < 0.05$). The highest ratio of *nirS*/(*nosZ*I + *nosZ*II) gene was observed at GP7 (0.06), while the lowest was observed in GP8 (Fig. 1e, green dots). Similar to the distribution of *nirS* gene abundance, the abundance of anammox bacteria increased slightly with sediment depth to the highest value at GP7 (2.58×10^5 copies g^{-1}) within the AATZ (Fig. 1d, purple bars). Anammox bacterial abundances in bottom sediments (GP8–10) were below the qPCR detection limit.

3.3. Potential N loss rates by denitrification and anammox

Potential denitrification rates, measured by ^{15}N isotope tracer method, ranged from 0.01 to 0.38 nmol N g^{-1} h^{-1} (Fig. 1c, red line). In line with the distribution pattern of denitrification abundances, highest potential denitrification rate was observed at GP7 within the AATZ and lower rates were seen in bottom sediments (GP8–10). Potential anammox rates ranged from 0 to 0.30 nmol N g^{-1} h^{-1}(Fig. 1d, orange line). Similarly, potential anammox rates peaked in GP7. Anammox rates of GP8–10 were below the detection limit. Denitrification contributed 29.3 to 95.3% of the total N_2 production in all samples, while anammox contributed nearly 50% of the total N_2 production in GP1–5. In the AATZ (GP6–7), potential N loss rates were higher than other sediment layers and denitrification was the dominant microbiological N loss pathway. In

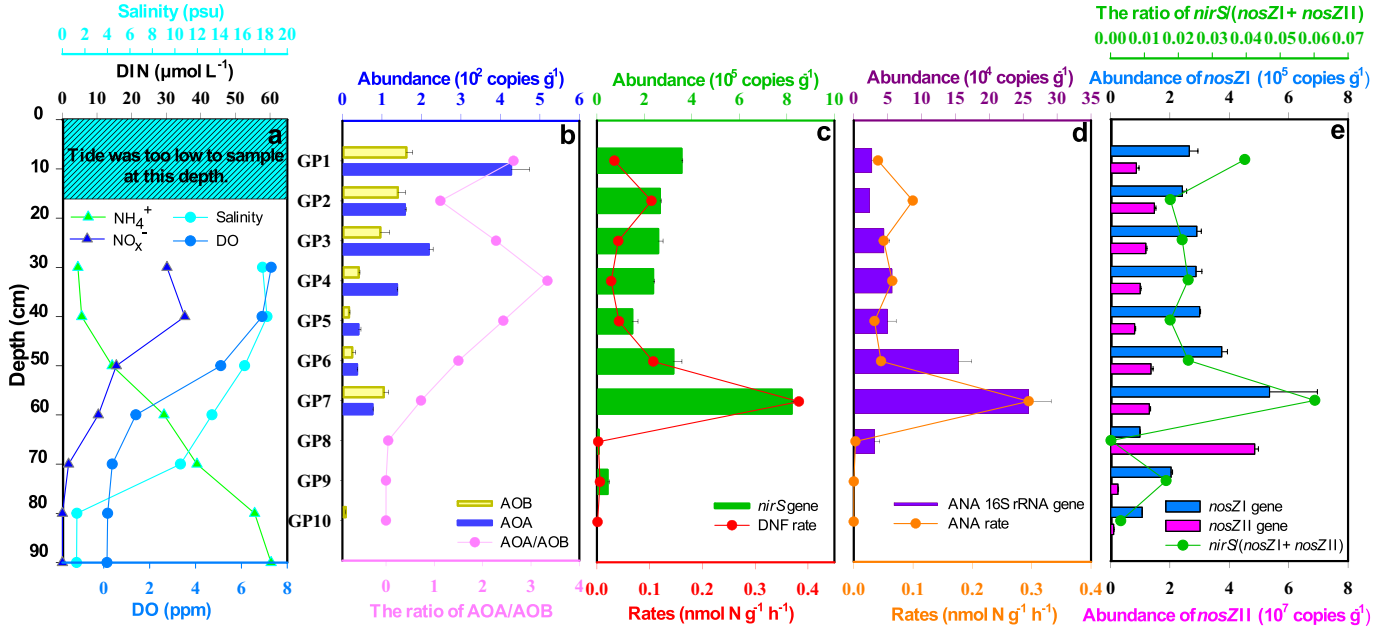

Fig. 1. Environmental parameters and microbial characteristics measured at different sediment core sampling depths. Vertical sections of the sediment core resulted in a total of 10 subsamples (GP1–10). (a) Vertical profiles of NH_4^+ and NO_x^- contents and salinity and DO (reported by Hong et al., 2019b) in groundwater. Tide was too low to sample the ground water in surface sediment (0–25 cm), so the groundwater samples of surface sediments were missing. (b) The abundances of ammonia-oxidizing bacteria (AOB: yellow bars, 10^5 copies g^{-1}) and archaea (AOA: blue bars, 10^5 copies g^{-1}) and ratios of AOA/AOB abundance (pink dots) in sediment core. (c) The potential rates (red line) and *nirS* gene abundances of denitrifiers (green bars, 10^5 copies g^{-1}) in sediment core. (d) The potential rates (orange line) and abundances of anammox bacteria (purple bars, 10^4 copies g^{-1}) in sediment core. (e) The abundances of *nosZ*I (sky blue bars, 10^5 copies g^{-1}) and *nosZ*II (dark pink bars, 10^7 copies g^{-1}) and ratios of *nirS*/(*nosZ*I + *nosZ*II) (light green dots) in sediment core. Horizontal bars denote standard error of triplicate samples. (For interpretation of the references to colour in this figure legend, the reader is referred to the web version of this article.)

general, a hotspot of N loss in the AATZ was evidenced by the highest activities and abundances of *nirS* and *nosZ*I and anammox bacteria in the GP-STE.

3.4. *nirS*-denitrifier bacterial community in sediment core

Samples GP8–10 could not be amplified by *nirS* gene targeted PCR due to low denitrifier abundances. A total of 140,000 denitrification raw sequences (20,000 sequences per sample) were run for denoising and trimming sequences. About 17,000 reads per sample of denitrification sequences were filtered as high-quality reads (Table 1). Seven samples generated about 715 OTUs (456 OTUs per sample) for the *nirS* gene of denitrification bacteria, with a Good's coverage of 0.99 at 97% similarly, providing information that OTUs of each denitrifying bacterial library had been captured effectively (Fig. S1a). Chao1 and ACE diversity indicators for denitrifiers ranged from 448.58 to 538.15 and 440.43 to 545.95, respectively. The Simpson diversity and Shannon richness ranged from 0.03 to 0.08 and 4.14 to 4.60, respectively. Evenness of denitrifiers was high, ranging from 0.67 to 0.75, suggesting that the community composition of *nirS* carrying denitrifiers (*nirS*-denitrifiers) remained relatively even within the GP-STE depths. The diversity of *nirS*-denitrifiers varied insignificantly along the sediment depth ($p > 0.05$).

The dominant OTUs of *nirS*-denitrifiers in the collected samples were phylogenetically affiliated with 10 different clusters, the relative abundances of cluster 1 through cluster 10 were 33.35%, 3.44%, 9.92%, 3.76%, 1.85%, 5.89%, 4.66%, 24.11%, 3.95% and 9.07%, respectively (Fig. 2a). The composition of *nirS*-denitrifiers varied significantly along the sediment depths. Cluster 1 is the dominant community of denitrifiers, especially in the surface sediment (GP1–4). As sediment depth increased, the relative abundance of Cluster 1 decreased and Clusters 6, 7 and 10 dominated the community in the bottom sediment (GP5–7). Compared to surface sediments, the diversity and composition of *nirS*-denitrifiers is less diverse in the AATZ. Obvious vertical distribution of community composition was also revealed by PCoA analysis (Fig. 2b). The first two principal coordinates explained 86.34% of the variance in the *nirS*-denitrifier community structure among all samples. The surface sediment assemblage (GP1–4, Group 1) of denitrifiers was distinct from the communities of GP5, GP6, and GP7, respectively. Fig. 2c shows a heat-map analysis of 50 selected dominant OTUs across all samples. OTU01 was the most dominant sequence in GP1–4. GP4 had highest number of dominant OTUs (46 OTUs), whereas the lowest were detected at GP1 and GP7 (average = 41 OTUs, $n = 7$). 28 dominant OTUs were cosmopolitan OTUs commonly present in all seven sediment samples. In comparison OTU21 and OTU47 were only observed in AATZ samples. Phylogenetic analysis of the TOP 50 OTUs was shown in Figs. 2d and S3. Cluster 1, contained the maximal amount of dominant denitrification OTUs, was affiliated to *Acidithiobacillia* and an uncultured bacterium found in the northwestern Pacific (AJ248412), while Cluster 2 was close related to *Sedimenticola thiotaurini* and an uncultured wetland bacterium (DQ767855). Cluster 3 was affiliated with *Sulfuricaulis limicola*, and an uncultured bacterium found in estuarine ecosystems (LJTT01000014). Cluster 4 was closely related to *Pseudomonas xanthomarina* and river sediment (KJ777998). Clusters 5, 6 and 7 were related to an uncultured bacterium observed in sediments of the Pearl River Estuary, soils in Zoige Plateau (KT783447) and marine sediments (LAZR01000648). Cluster 8 was affiliated to *Bradyrhizobium* and an uncultured bacterium from the Amundsen Sea (KP723703 and KP723725), the Black Sea (DQ479841) and the San Francisco Bay (KR061015). Cluster 9 was related to an uncultured bacterium from the Arabian Sea (AY336807), while Cluster 10 was affiliated to *Nitratiruptor*. All of the 10 clusters belonged to *Proteobacteria*. In addition, Clusters 2 and 4 were affiliated to the γ subdivision of *proteobacteria*, while Clusters 3, 8 and 10 were closely related to the β-, α- and ε- subdivisions of *proteobacteria*.

3.5. Anammox bacterial community in sediment core

Sample GP1 could not be successfully amplified by anammox specific-16S rRNA gene targeted PCR, so we do not know the diversity and community composition of anammox bacteria in GP1. About 180,000 anammox bacterial raw sequences (20,000 sequences per sample) were run for denoising and trimming sequences. A total of 14,000 reads per sample of anammox bacterial sequences were filtered as high-quality reads (Table 1). About 250 OTUs (141 OTUs per sample) for anammox bacteria were generated by nine samples. A Good's coverage of 0.99 at 97% suggested that OTUs of each anammox bacterial library had been captured effectively (Fig. S1b). Chao1 and ACE diversity indicators for anammox bacteria ranged from 130.69 to 228.05 and 135.43 to 210.38, respectively. The Simpson diversity and Shannon richness ranged from 0.04 to 0.08 and 3.48 to 3.78, respectively. Evenness of anammox bacteria was high, ranging from 0.70 to 0.76, suggesting that the community composition of anammox bacteria was quite even across all the samples. The alpha diversity of anammox bacteria in the AATZ was higher than other sediment depths. Compared to *nirS*-denitrifiers, the diversity of the anammox bacterial community was much lower and simpler.

The dominant anammox bacterial OTUs, with 97% similarity, in all samples were affiliated to three genera, including *Ca*. Brocadia (58.00%), *Ca*. Kuenenia (9.50%), and *Ca*. Scalindua (28.29%) (Fig. 3a). In addition, one unknown genus was also detected (4.22%). *Ca*.

Table 1
Estimates of denitrification *nirS* gene and anammox specific-16S rRNA gene sequences richness and diversity in different sediment.

Genes	Samples	High quality sequences	OTU[a]	Chao1[a]	ACE[a]	Shannon[a]	Evenness[b]	Simpson	Coverage
Denitrification *nirS* gene	GP1	17,521	444	481.65	470.65	4.48	0.73	0.04	0.996
	GP2	17,326	475	506.40	504.78	4.60	0.75	0.04	0.996
	GP3	17,031	473	514.13	511.24	4.14	0.67	0.08	0.995
	GP4	16,831	502	538.15	545.95	4.24	0.68	0.06	0.995
	GP5	16,568	433	462.50	464.17	4.21	0.69	0.05	0.996
	GP6	16,609	469	518.76	500.32	4.59	0.75	0.03	0.996
	GP7	17,178	401	448.58	440.43	4.29	0.72	0.04	0.996
Anammox specific-16S rRNA gene	GP2	13,906	125	130.69	135.43	3.52	0.73	0.05	0.999
	GP3	14,805	130	150.13	147.85	3.56	0.73	0.05	0.998
	GP4	14,377	138	186.77	178.05	3.72	0.76	0.04	0.998
	GP5	14,102	148	171.87	177.70	3.78	0.76	0.04	0.998
	GP6	15,641	159	193.91	188.76	3.72	0.73	0.05	0.998
	GP7	14,101	146	228.05	210.38	3.65	0.73	0.04	0.998
	GP8	14,549	152	174.25	174.07	3.52	0.70	0.08	0.998
	GP9	14,035	139	172.19	167.90	3.48	0.70	0.06	0.998
	GP10	14,739	137	162.10	157.02	3.58	0.73	0.05	0.998

[a] Richness and diversity were determined based on 0.03 distance.
[b] Evenness was calculated by dividing Shannon index by Ln(OTUs).

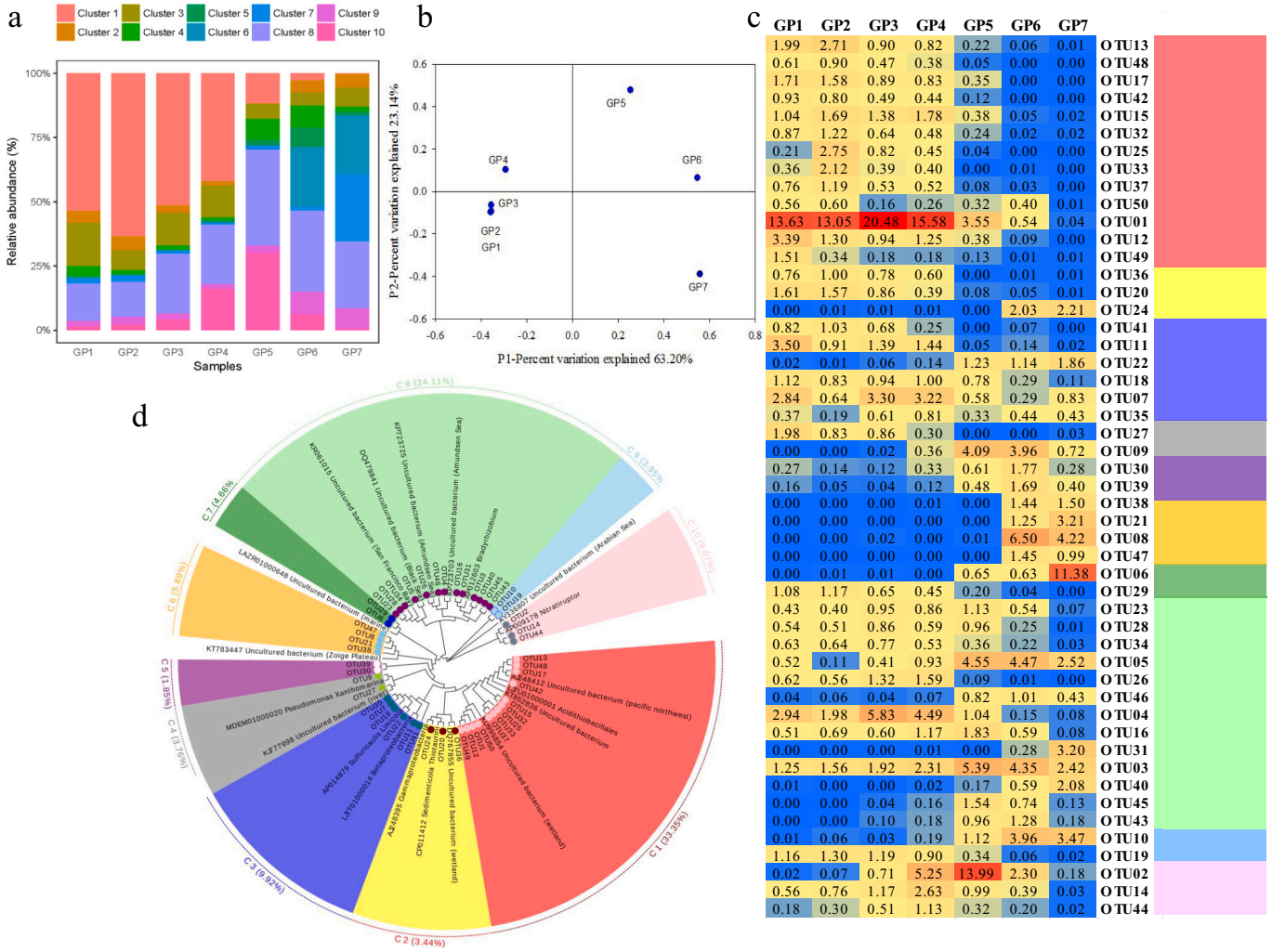

	GP1	GP2	GP3	GP4	GP5	GP6	GP7	
OTU13	1.99	2.71	0.90	0.82	0.22	0.06	0.01	OTU13
OTU48	0.61	0.90	0.47	0.38	0.05	0.00	0.00	OTU48
OTU17	1.71	1.58	0.89	0.83	0.35	0.00	0.00	OTU17
OTU42	0.93	0.80	0.49	0.44	0.12	0.00	0.00	OTU42
OTU15	1.04	1.69	1.38	1.78	0.38	0.05	0.02	OTU15
OTU32	0.87	1.22	0.64	0.48	0.24	0.02	0.02	OTU32
OTU25	0.21	2.75	0.82	0.45	0.04	0.00	0.00	OTU25
OTU33	0.36	2.12	0.39	0.40	0.00	0.01	0.00	OTU33
OTU37	0.76	1.19	0.53	0.52	0.08	0.03	0.00	OTU37
OTU50	0.56	0.60	0.16	0.26	0.32	0.40	0.01	OTU50
OTU01	13.63	13.05	20.48	15.58	3.55	0.54	0.04	OTU01
OTU12	3.39	1.30	0.94	1.25	0.38	0.09	0.00	OTU12
OTU49	1.51	0.34	0.18	0.18	0.13	0.01	0.01	OTU49
OTU36	0.76	1.00	0.78	0.60	0.00	0.01	0.01	OTU36
OTU20	1.61	1.57	0.86	0.39	0.08	0.05	0.01	OTU20
OTU24	0.00	0.01	0.01	0.01	0.00	2.03	2.21	OTU24
OTU41	0.82	1.03	0.68	0.25	0.00	0.07	0.00	OTU41
OTU11	3.50	0.91	1.39	1.44	0.05	0.14	0.02	OTU11
OTU22	0.02	0.01	0.06	0.14	1.23	1.14	1.86	OTU22
OTU18	1.12	0.83	0.94	1.00	0.78	0.29	0.11	OTU18
OTU07	2.84	0.64	3.30	3.22	0.58	0.29	0.83	OTU07
OTU35	0.37	0.19	0.61	0.81	0.33	0.44	0.43	OTU35
OTU27	1.98	0.83	0.86	0.30	0.00	0.00	0.03	OTU27
OTU09	0.00	0.00	0.02	0.36	4.09	3.96	0.72	OTU09
OTU30	0.27	0.14	0.12	0.33	0.61	1.77	0.28	OTU30
OTU39	0.16	0.05	0.04	0.12	0.48	1.69	0.40	OTU39
OTU38	0.00	0.00	0.00	0.01	0.00	1.44	1.50	OTU38
OTU21	0.00	0.00	0.00	0.00	0.00	1.25	3.21	OTU21
OTU08	0.00	0.00	0.02	0.00	0.01	6.50	4.22	OTU08
OTU47	0.00	0.00	0.00	0.00	0.00	1.45	0.99	OTU47
OTU06	0.00	0.01	0.01	0.00	0.65	0.63	11.38	OTU06
OTU29	1.08	1.17	0.65	0.45	0.20	0.04	0.00	OTU29
OTU23	0.43	0.40	0.95	0.86	1.13	0.54	0.07	OTU23
OTU28	0.54	0.51	0.86	0.59	0.96	0.25	0.01	OTU28
OTU34	0.63	0.64	0.77	0.53	0.36	0.22	0.03	OTU34
OTU05	0.52	0.11	0.41	0.93	4.55	4.47	2.52	OTU05
OTU26	0.62	0.56	1.32	1.59	0.09	0.01	0.00	OTU26
OTU46	0.04	0.06	0.04	0.07	0.82	1.01	0.43	OTU46
OTU04	2.94	1.98	5.83	4.49	1.04	0.15	0.08	OTU04
OTU16	0.51	0.69	0.60	1.17	1.83	0.59	0.08	OTU16
OTU31	0.00	0.00	0.00	0.01	0.00	0.28	3.20	OTU31
OTU03	1.25	1.56	1.92	2.31	5.39	4.35	2.42	OTU03
OTU40	0.01	0.00	0.00	0.02	0.17	0.59	2.08	OTU40
OTU45	0.00	0.00	0.04	0.16	1.54	0.74	0.13	OTU45
OTU43	0.00	0.00	0.10	0.18	0.96	1.28	0.18	OTU43
OTU10	0.01	0.06	0.03	0.19	1.12	3.96	3.47	OTU10
OTU19	1.16	1.30	1.19	0.90	0.34	0.06	0.02	OTU19
OTU02	0.02	0.07	0.71	5.25	13.99	2.30	0.18	OTU02
OTU14	0.56	0.76	1.17	2.63	0.99	0.39	0.03	OTU14
OTU44	0.18	0.30	0.51	1.13	0.32	0.20	0.02	OTU44

Fig. 2. Microbial characteristics of the denitrification *nirS* gene in the sediment core. (a) Relative abundance of 10 clusters of denitrifiers based on OTUs at a 97% sequence identity cut-off. (b) The principal coordinates (PCoA) analyses for *nirS*-denitrifiers retrieved from sediments. (c) The heat map of the most abundant *nirS* OTUs (Top 50 OTUs, 97% cutoff). (d) Neighbor-joining phylogenetic tree of the dominant (Top 50 OTUs) denitrification OTUs and the reference sequences from GenBank. Bootstrap values were 1000 replicates.

Brocadia was the most abundant genus and the Unknown was the rarer genus across the samples. The composition of anammox bacteria varied insignificantly with the sediment depth. PCoA was used to analyze the difference of community composition among all the samples (Fig. 3b). The first two principal coordinates explained 79.17% of the variance in the anammox bacterial community among all samples. The surface sediment assemblage (GP2–5) and GP10 of anammox bacteria were distinct from the communities of GP6, GP7, GP8 and GP9, respectively. The community composition of anammox bacteria in the AATZ differs from other samples.

Fig. 3c shows the heat-map analysis of 28 selected dominant OTUs across all samples. GP6 had highest number of dominant OTUs (30 OTUs), whereas the lowest were detected at GP2, GP4 and GP9 (27 OTUs). 23 of the dominant OTUs were cosmopolitan and commonly present in all nine sediment samples, but OTU05 was the most abundant group of sequences in GP8 (9.36). Phylogenetic analysis of TOP 30 OTUs is shown in Figs. 3d and S4. OTU01, closely related to *Ca.* Brocadia, was the most abundant member in GP1–4. 14 OTUs belong to *Ca.* Brocadia. In addition to *Ca.* Brocadia fulgida (EU478693), *Ca.* Brocadia caroliniensis (JF487828), *Ca.* Brocadia sapporoensis (KY659581), *Ca.* Brocadia anammoxidans (AF375994), *Ca.* Brocadia sinica (AB565477) and *Ca.* Brocadia brasiliensis (GQ896513) were also detected in the sediments. OTU06 and OTU11 were affiliated to *Ca.* Kuenenia stuttgartiensis (AF375995). OTU05, affiliated to *Ca.* Scalindua, was the most abundant member in GP6 and GP8. 11 OTUs were closely related to *Ca.* Scalindua wagneri (AY254882), *Ca.* Scalindua japonica (AB573103), *Ca.* Scalindua Arabica (EU478624), *Ca.* Scalindua brodae (AY254883), *Ca.* Scalindua sorokinii (AY257181) and *Ca.* Scalindua marina (EF602038). Three OTUs, including OTU30, OTU15 and OTU17, were not affiliated to any known anammox genera.

3.6. Correlation analysis between microbial characteristics and sediment properties

The relationship between activities, abundance, community composition of microbial N loss community and the sediment properties were analyzed by Pearson correlation analysis (Table S2) and redundancy analysis (RDA, Fig. S2a and b). The salinity, DO, ORP, pH, N_2O, Fe concentrations reported by Hong et al. (2019b) and the concentrations of Mn, humid acid, and SO_4^{2-} measured by Beck et al. (2016) were used for the correlation analysis. Salinity and DO in groundwater negatively correlated with depth, NH_4^+, and positively correlated with NO_x^-, AOA and AOB abundances. The characteristics of denitrifiers (the abundances of *nirS* and *nosZ*I gene and denitrification rates) positively correlated with anammox bacteria (the abundances of anammox specific-16S rRNA gene and anammox rates). *nosZ*II gene abundance positively correlated

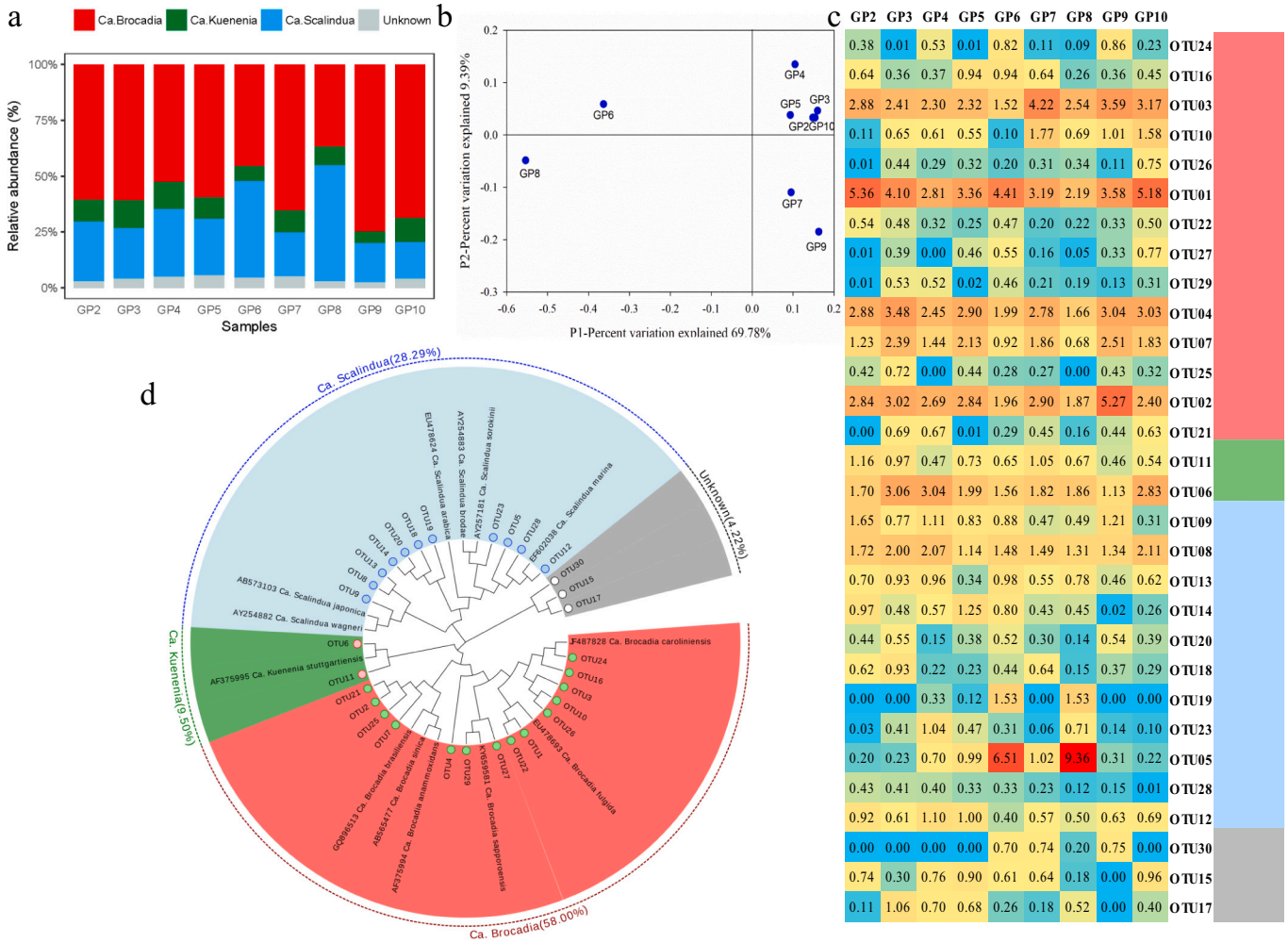

Fig. 3. Microbial characteristics of the anammox 16S rRNA gene in the sediment core. (a) Relative abundance of different anammox genera based on OTUs at a 97% sequence identity cut-off. (b) The PCoA analyses for anammox 16S rRNA gene sequences retrieved from sediments. (c) The heat map of the most abundant anammox OTUs (Top 30 OTUs, 97% cutoff). (d) Neighbor-joining phylogenetic tree of the dominant (Top 30 OTUs) anammox OTUs and the reference sequences from GenBank. Bootstrap values were 1000 replicates.

with Fe II concentration. N_2O positively correlated with denitrification rate and abundance of *nirS* and anammox specific-16S rRNA genes. There were not significant relationships between N_2O and NO_x^- and NH_4^+. The ratio of *nirS*/(*nosZ*I + *nosZ*II) negatively correlated with depth, and positively correlated with NO_x^-, AOA and AOB abundances, salinity, DO and pH.

As revealed by RDA, the first two RDA axes explained 92.03% and 58.20% of the cumulative variance of the denitrification and anammox bacterium-environment relationship, respectively (Fig. S2a and b). The community compositions of denitrifiers based on *nirS* gene were affected by depth, salinity, DO, ORP, pH, NOx^-, NH_4^+, N_2O, and Fe. No factor was shown to have a significant effect on the anammox community.

4. Discussion

4.1. Microbial characteristics of N loss processes in STE

The distribution and activities of denitrification and anammox have been investigated by molecular ecological analyses and ^{15}N-tracer incubations in various ecosystems, including: estuaries (Wu et al., 2020; Xie et al., 2020), bays (Liu et al., 2020; Wu et al., 2019b), mangrove wetlands (Xiao et al., 2018), intertidal zones (Jiao et al., 2018) and red soils (Wu et al., 2018). Using a similar method, we firstly reported the vertical characteristics of denitrification and anammox in a permeable STE. In this study, the denitrification *nirS* gene abundance (10^5 copies g^{-1}) and potential rate (0.01–0.38 nmol N g^{-1} h^{-1}) in STE were lower than the reported values of intertidal marsh (Zheng et al., 2016a), estuarine (Xie et al., 2020), bay (Liu et al., 2020) and freshwater sediments (Gao et al., 2016; Zhu et al., 2013). Sandy subterranean is often low in organic carbon (Santoro, 2010). Most denitrifiers are heterotrophic organisms, so the availability of organic matter is a major factor influencing the activity and abundance of denitrifiers in low-carbon STE environments (Santoro, 2010). The anammox bacterial abundance (10^4 copies g^{-1}) and potential rate (0–0.30 nmol N g^{-1} h^{-1}) were in the relatively wide range of those previously detected in estuarine (Lisa et al., 2014; Wu et al., 2020; Zheng et al., 2016b), bay (Wu et al., 2019b), and freshwater sediments (Shen et al., 2017; Zhu et al., 2013). N_2 production by denitrification exceeded that from anammox as the dominant N loss process in both low and high permeable sediment as observed in previous studies (Gao et al., 2012; Marchant et al., 2016; Rao et al., 2008). Nevertheless, the contributions to N loss of denitrification and anammox were almost equal in STE (nearly 50%). Based on the denitrification and anammox rates, the sediment N loss in this study was estimated at 13.15 mmol N m^{-3} day^{-1}.

10 different clusters of *nirS*-denitrifiers were shown in Fig. 2a, which all belonged to *Proteobacteria*. Cluster 2 and 4 were related to γ-*proteobacteria*, while cluster 3, 8 and 10 were affiliated to β-, α- and ε- *proteobacteria*. Cluster 1 belonged to *Acidithiobacillia*. In line with the *nirS*-

denitrifier community in permeable sediments of the Wadden Sea, most reads were associated with γ-, β-, α- and ε- *proteobacteria* (Marchant et al., 2018). The results of dominant anammox bacterial OTUs were similar to other land-sea transition zones, such as an estuary (Wu et al., 2020), a bay (Wu et al., 2019b) and a low permeable intertidal zone (Jiao et al., 2018) (Fig. 3a). To our knowledge, this study is the first to report the anammox community composition by high-throughput sequencing analysis in a highly permeable STE. The high diversity of anammox bacteria observed at land-sea transition zones may be due to the complexity of the environment and the mixing of river runoff or, in our case, groundwater with the tidal current (Wang et al., 2015). Recently, Ahmerkamp et al. (2020) found that sand gains with a golf-ball like structure are ideal for microbial colonization by providing protective structures as well as ensuring an optimal solute supply. This may explain the diverse microbial N loss communities observed in the high permeable, sandy STE.

Along the sediment depth, the highest bacterial abundance and potential rates of denitrification and anammox were observed in GP7, which was within the AATZ (Fig. 1b and c). In comparison to other depths, this was identified as a hotspot of N loss in the AATZ (55–60 cm in depth). Consistent with the predicted microbial functions reported by Hong et al. (2019b), AATZ could support a wide variety of biogeochemical processes with complex predicted microbial potential functions. Previous studies have reported that the intertidal beach sands host high rates of N cycling processes (nitrification, denitrification and anammox) and are a sink for bioavailable N (Ahrens et al., 2020; Couturier et al., 2017). Denitrification hotspots have also been identified by model simulations (Heiss et al., 2020) and field observations (Kim et al., 2017, 2019; Schutte et al., 2015) of intertidal sandy beaches.

Above the AATZ, NO_x^- was the dominant form of DIN, whereas the NH_4^+ concentrations were lower than those in other zones (Fig. 1a). DO and ORP profiles showed that active brackish water and groundwater exchange promotes DO penetration to reach 60 cm depth (Hong et al., 2019b). The abundances of AOA ($r = -0.87$, $p < 0.01$) and AOB ($r = -0.82$, $p < 0.01$) decreased with sediment depth (Fig. 1d), suggesting that nitrification process is active in surface sediment where DO is available. Schutte et al. (2018) found elevated NO_3^- concentrations and deep DO penetration drives active nitrification in permeable sandy beach sediment. Denitrification and anammox are inhibited under oxic conditions, though aerobic denitrification has been observed in some intertidal zones (Gao et al., 2010). In addition, DOC was relatively low (320 μM) in the surface groundwater of Gloucester Beach (O'Connor et al., 2015). So denitrification may have been limited by low DOC concentrations above the AATZ.

In the AATZ, NH_4^+ was the dominant form of DIN (Fig. 1a) and sharply decreasing concentrations of DO and ORP were observed (Hong et al., 2019b). The AOP abundances (AOA and AOB) decreased with sediment depth (Fig. 1d). In addition, a positive correlation between AOP abundances and redox indicators (DO and ORP) and NOx^- contents were observed (Table S2). This suggests that vertical dispersion of NO_x^- driven by surface brackish water and groundwater exchange may support the observed hotspot of denitrification and anammox in the AATZ. Aller (1994) found that the rapid changes in the oxidation-reduction conditions stimulated the coupling between nitrification and denitrification in sediments. The infiltration of O_2 in the beach drives nitrification in STE, providing the NO_2^- and NO_3^- for denitrification and anammox (Schutte et al., 2018). Groundwater rich with NH_4^+ may be expected to support anammox in the AATZ. In addition, O'Connor et al. (2015) found maximum dissolved Fe concentration (30 μM) were observed between 50 and 60 depth. Higher Fe contents in AATZ may accumulate the abundance and activities of nitrite oxide reductases because *nirS* is an iron containing cd1-type reductase (Saarenheimo et al., 2015). Furthermore, low DO conditions in the AATZ would stimulate N loss pathways, especially NO_3^- attenuation by denitrification. Previous studies shown that DO is one of the most important factors affecting N loss in coastal water and sediments (Hong et al., 2019b; Körner and Zumft, 1989; Lin et al., 2016). Xiao et al. (2018) found that seawater and groundwater exchange facilitated high-oxygen seawater infiltration and subsequent nitrification in tidal creeks.

O'Connor et al. (2015) reported that DOC increased rapidly to 2.9 mM at 50–100 cm depth and humic carbon made up 43% of total DOC in the sediments of GP-STE. Most denitrifiers are heterotrophic organisms, so higher DOC and humic carbon may support denitrification in the AATZ. Lovley et al. (1999) found that heterotrophic denitrifying bacterium *Paracoccus denitrificans* can oxidize humic acids coupled to nitrate reduction. Recent study also reported that humic substance can act as an electron shuttle for anaerobic methane oxidation (AMO) coupled to N_2O reduction in wetland sediments (Valenzuela et al., 2020). In addition, the STE has a long residence time (46 day, O'Connor et al. (2015)), which creates a favorable environment for N loss by the coupling of nitrification and denitrification or anammox in the AATZ. Under low oxygen conditions where groundwater and seawater are mixed, microbes can alternate or simultaneously carry out aerobic and anaerobic respiration (Hong et al., 2019b). Thus, microbial efficiency of metabolic productivity would be higher in the AATZ (Zannoni, 2004).

Below the AATZ, the lowest abundances of AOB, AOA, denitrifying (based on *nirS* and nosZI genes) and anammox bacteria, as well as activities of denitrification and anammox were observed (Fig. 1b, c, and d). NH_4^+ was the dominant form of DIN, whereas NO_X^- was below the detection limit (Fig. 1a). O'Connor et al. (2015) also found that NO_3^- was low in porewater of deeper sediments of the Gloucester Point Beach. NO_X^- availability is limited by the inactive nitrification. NO_3^- is one of the most important factors limiting the denitrificaiton process in permeable tidal sediment (Marchant et al., 2016). Higher sulfide concentrations (>1000 μM) were reported below 75 cm depth (O'Connor et al., 2015), which have been shown to inhibit denitrification (Senga et al., 2006). The concentrations of NO_2^- were under the detection limit in the groundwater of GP-STE (<0.5 μM). Although there are high NH_4^+ concentrations in the groundwater, anammox activity is limited by NO_2^- availability. In addition, the low values of NO_2^- suggested that the activity of ammonia oxidation process was low or the NO_2^- produced by ammonia oxidation process maybe immediately transformed to N_2 by denitrification and anammox process.

Compared with surface sediments, the diversity and composition of *nirS*-denitrifiers tends to be less diverse in the AATZ. PCoA analysis also showed that the surface assemblage (GP1–4, Group 1) of *nirS*-denitrifiers was distinct from the communities of GP5, GP6, and GP7 (Fig. 3b). The communities of *nirS*-denitrifiers were shaped by the different geochemical conditions in the AATZ. RDA analysis showed that the communities of *nirS*-denitrifiers were affected by depth, salinity, DO, ORP, pH, NOx^-, NH_4^+, N_2O, and Fe (Fig. S2a). Vertical redox gradient (DO and ORP) significantly affected the community *nirS*-denitrifiers. *nirS*-denitrifiers adapted to the dynamic hydrological and geochemical conditions are selected for and dominate the community in the AATZ. In contrast with *nirS*-denitrifiers, *nosZ*I N_2O reducer and anammox bacteria were less sensitive to the dynamic hydrological and geochemical conditions in AATZ. PCoA analysis showed that the surface assemblage (GP2–5) and GP10 of anammox bacteria were distinct from the communities of GP6, GP7, GP8 and GP9, respectively. No geochemical factors were shown to have a significant effect on the anammox community (Fig. S2b).

4.2. Distribution pattern of N_2O reducing communities in STE

Denitrification (including bacterial denitrification, fungal denitrification and chemodenitrification) and nitrification processes are known to contribute to N_2O production, but the only known N_2O sink is the reduction to N_2 by microorganisms that possess the *nosZ*I or *nosZ*II genes encoding N_2O reductase (Jones et al., 2013). The net N_2O emission is partly determined by the balance between N_2O-producing denitrifiers (encoded by *nirS* or *nirK* genes) and N_2O-reducing denitrifiers (encoded by *nosZ*I and *nosZ*II genes). Graf et al. (2014) found that *nosZ*I clade were

more likely to be complete denitrifiers, in which NO_3^- or NO_2^- are reduced to N_2O and to N_2. In addition, 51% of the *nosZ*II clade appear to be nondenitrifying N_2O reducers that lacked the genetic capacity to produce N_2O.

In this study, the abundance of *nosZ*I and II genes of denitrifiers varied insignificantly with sediment depth ($p > 0.05$, GP1–6). But highest values were observed at GP7 and GP8, respectively (Fig. 1e). *nosZ*I abundances (10^5 copies g^{-1}) were lower than the reported values in a wetland (Ligi et al., 2015), a eutrophic lagoon (Highton et al., 2016), constructed wetlands (Paranychianakis et al., 2016), rhizosphere soils (Zhao et al., 2020) and agricultural soil (Juhanson et al., 2017). *nosZ*II abundances (10^7 copies g^{-1}) were within the relatively wide range of those previously measured in rhizosphere (Zhao et al., 2020) and agricultural soil (Juhanson et al., 2017), but lower than those observed in a wetland (Ligi et al., 2015) and a eutrophic lagoon (Highton et al., 2016). In this study, *nosZ*II abundances (10^7 copies g^{-1}) were two orders of magnitude higher than *nosZ*I and *nirS* abundances (10^5 copies g^{-1}). Graves et al. (2016) reported that the *nosZ*II gene was three times more abundant than *nosZ*I in salt marsh sediment based on metagenomic analysis. Several possible factors contribute to the unexpectedly high abundance of *nosZ*II in the STE. Compared to *nosZ*I N_2O reducers, Yoon et al. (2016) reported that *nosZ*II N_2O reducers have lower whole cell half-saturation constants for N_2O, giving them a competitive edge under conditions of low N_2O concentrations. Low N_2O concentrations, ranging from 0.06 to 0.13 ppm, were measured by Hong et al. (2019b) in GP-STE. Thus, low N_2O concentrations observed in the GP-STE may favor *nosZ*II N_2O reducers. In addition, *nosZ*II N_2O reducers produced 50–80% more biomass per mol of N_2O reduced and have more efficient free energy conservation compared to the *nosZ*I N_2O reducers (Yoon et al., 2016). Furthermore, the diversity of *nosZ*II N_2O reducers is typically higher than *nosZ*I (Jones et al., 2014; Wittorf et al., 2016). Higher diversity of *nosZ*II N_2O reducers may give them a competitive edge in adapting to the highly variable environments driven by brackish water and groundwater exchange in STE sediments. Jørgensen and Nelson (2004) reported that N_2O reduction encoded by *nosZ*II is known to be linked to respiratory ammonification. Conditions of fluctuating oxygen concentrations could be considered an advantage for organisms capable of facultative denitrification (Wittorf et al., 2016), supporting higher abundances of *nosZ*II denitrifiers in the AATZ of the GP-STE. There is no significant relationship between *nosZ*I and *nosZ*II abundances by correlation analysis ($r = -0.24$, $p > 0.05$, Table S2), suggesting that both *nosZ* genes have different patterns along the depth profiles. The distinct correlation between the clade I and II *nosZ* genes and the environmental parameters considered (Table S2) provides evidence that they occupy different ecological niches. To the best of our knowledge, this is the first study reporting *nosZ*I and *nosZ*II abundance in a STE.

5. Conclusions

This study highlights the N loss processes in sediments of the GP-STE. A hotspot of N loss was observed in the AATZ at 50–60 cm depth (GP6–7), which is evidenced by this depth exhibiting the highest observed activities, abundances, as well as diversity of denitrifiers and anammox bacteria. Denitrification and anammox played equal roles in N loss. *nosZ*II genes had high abundances (10^7 copies g^{-1}) and dominated the community of N_2O reducers along the sediment depth. Strong vertical brackish water and groundwater exchange accelerated the vertical dispersion of NO_x^- and created redox gradients that promoted the coupling of nitrification and denitrification and anammox to remove fixed N in the AATZ of the GP-STE. Overall, a multidisciplinary study of geochemistry, isotope tracer incubation methods, and microbial molecular ecology were employed to highlight the role of coupled nitrification to denitrification and anammox allowing for attenuation of reactive Ns discharging from the STE to surrounding estuaries and coasts. A more thorough understanding of spatial and temporal variation in N loss (denitrification and anammox) activities, abundances and community composition are required to further understand the role of N cycling in STEs.

CRediT authorship contribution statement

Jiapeng Wu: Conceptualization, Investigation, Methodology, Writing – Original draft preparation.

Yiguo Hong: Methodology, Writing – Reviewing & Editing, Supervision.

Stephanie Wilson: Methodology, Visualization.

Bongkeun Song: Sampling, Writing – Reviewing & Editing, Supervision.

Declaration of competing interest

The authors declare that they have no known competing financial interests or personal relationships that could have appeared to influence the work reported in this paper.

Acknowledgments

We would like to thank the financially supported by the National Science Foundation of China (No. 31870100, No. 42006122 and No. 91851111), Natural Science Foundation of Guangdong Province (2021A1515011548), Basic and Applied Basic Research Foundation of Guangdong Province (No. 2020A1515110597 and No. 2019B1515120066), Young Talent Research Project of Guangzhou Education Bureau (No. 202032795) and the US National Science Foundation (OCE1658135). We acknowledge Michele Cochran for groundwater sampling and geochemical measurements and Dr. Christopher Hein for aid with vibracore sediment sampling.

Appendix A. Supplementary data

Supplementary data to this article can be found online at https://doi.org/10.1016/j.marpolbul.2021.112440.

References

Addy, K., Gold, A., Nowicki, B., Mckenna, J., Stolt, M., Groffman, P., 2005. Denitrification capacity in a subterranean estuary below a Rhode Island fringing salt marsh. Estuaries 28, 896–908.

Ahmerkamp, S., Marchant, H.K., Peng, C., Probandt, D., Littmann, S., Kuypers, M.M.M., Holtappels, M., 2020. The effect of sediment grain properties and porewater flow on microbial abundance and respiration in permeable sediments. Sci. Rep. 10, 3573.

Ahrens, J., Beck, M., Marchant, Hannah K., Ahmerkamp, S., Schnetger, B., Brumsack, H.-J., 2020. Seasonality of organic matter degradation regulates nutrient and metal net fluxes in a high energy sandy beach. J. Geophys. Res. Biogeosci. 125, e2019JG005399.

Aller, R.C., 1994. Bioturbation and remineralization of sedimentary organic matter: effects of redox oscillation. Chem. Geol. 114, 331–345.

Beck, A.J., Kellum, A.A., Luek, J.L., Cochran, M.A., 2016. Chemical flux associated with spatially and temporally variable submarine groundwater discharge, and chemical modification in the subterranean estuary at Gloucester Point, VA (USA). Estuar. Coasts 39, 1–12.

Beusen, A.H.W., Slomp, C.P., Bouwman, A.F., 2013. Global land–ocean linkage: direct inputs of nitrogen to coastal waters via submarine groundwater discharge. Environ. Res. Lett. 8, 034035.

Charette, Sholkovitz, 2002. Oxidative precipitation of groundwater-derived ferrous iron in the subterranean estuary of a coastal bay. Geophys. Res. Lett. 29, 85-81-85-84.

Cho, H.-M., Kim, G., Kwon, E.Y., Moosdorf, N., Garcia-Orellana, J., Santos, I.R., 2018. Radium tracing nutrient inputs through submarine groundwater discharge in the global ocean. Sci. Rep. 8, 2439.

Couturier, M., Tommi-Morin, G., Sirois, M., Rao, A., Nozais, C., Chaillou, G., 2017. Nitrogen transformations along a shallow subterranean estuary. Biogeosciences 14, 3321–3336.

Dalsgaard, T., Thamdrup, B., 2002. Factors controlling anaerobic ammonium oxidation with nitrite in marine sediments. Appl. Environ. Microbiol. 68, 3802–3808.

Francis, C.A., Roberts, K.J., Beman, J.M., Santoro, A.E., Oakley, B.B., 2005. Ubiquity and diversity of ammonia-oxidizing archaea in water columns and sediments of the ocean. Proc. Natl. Acad. Sci. U. S. A. 102, 14683–14688.

Gao, H., Matyka, M., Liu, B., Khalili, A., Kostka, J.E., Collins, G., Jansen, S., Holtappels, M., Jensen, M.M., Badewien, T.H., Beck, M., Grunwald, M., de Beer, D.,

Lavik, G., Kuypers, M.M.M., 2012. Intensive and extensive nitrogen loss from intertidal permeable sediments of the Wadden Sea. Limnol. Oceanogr. 57, 185–198.
Gao, J., Hou, L., Zheng, Y., Liu, M., Yin, G., Li, X., Lin, X., Yu, C., Wang, R., Jiang, X., Sun, X., 2016. nirS-encoding denitrifier community composition, distribution, and abundance along the coastal wetlands of China. Appl. Microbiol. Biotechnol. 100, 8573–8582.
Gao, H., Schreiber, F., Collins, G., Jensen, M.M., Kostka, J.E., Lavik, G., De, B.D., Zhou, H., Mmm, K., 2010. Aerobic denitrification in permeable Wadden Sea sediments. ISME J. 4, 417–426.
Gonneea, Charette, 2014. Hydrologic controls on nutrient cycling in an unconfined coastal aquifer. Environ. Sci. Technol. 48, 14178–14185.
Graf, D.R.H., Jones, C.M., Hallin, S., 2014. Intergenomic comparisons highlight modularity of the denitrification pathway and underpin the importance of community structure for N2O emissions. PLoS One 9, e114118.
Graves, C.J., Makrides, E.J., Schmidt, V.T., Giblin, A.E., Cardon, Z.G., Rand, D.M., 2016. Functional responses of salt marsh microbial communities to long-term nutrient enrichment. Appl. Environ. Microbiol. 82, 2862–2871.
Guan, F., Hong, Y., Jiapeng, W., Wang, Y., Liying, B., Tang, B., Xie, G., 2017. A fast sodium hypobromite oxidation method for the sequential determination of ammonia nitrogen in small volume. Ecol. Sci. 36 (2), 42–48.
Heiss, J., Holly, M., Mohammad, K., 2020. Denitrification hotspots in intertidal mixing zones linked to geologic heterogeneity. Environ. Res. Lett. 15, 084015.
Highton, M.P., Stéphanie, R., Josie, C., Marc, S., Morales, S.E., 2016. Physical factors correlate to microbial community structure and nitrogen cycling gene abundance in a nitrate fed eutrophic lagoon. Front. Microbiol. 7, 1691.
Hong, Y., Wu, J., Guan, F., Yue, W., Long, A., 2019a. Nitrogen removal in the sediments of the Pearl River Estuary, China: evidence from the distribution and forms of nitrogen in the sediment cores. Mar. Pollut. Bull. 138, 115–124.
Hong, Y., Wu, J., Wilson, S., Song, B., 2019b. Vertical stratification of sediment microbial communities along geochemical gradients of a subterranean estuary located at the Gloucester Beach of Virginia, United States. Front. Microbiol. 9, 3343.
Jiao, L., Wu, J., He, X., Wen, X., Li, Y., Hong, Y., 2018. Significant microbial nitrogen loss from denitrification and anammox in the land-sea interface of low permeable sediments. Int. Biodeterior. Biodegradation 135, 80–89.
Jones, C.M., Graf, D.R.H., Bru, D., Philippot, L., Hallin, S., 2013. The unaccounted yet abundant nitrous oxide-reducing microbial community: a potential nitrous oxide sink. ISME J. 7, 417–426.
Jones, C.M., Spor, A., Brennan, F.P., Breuil, M.-C., Bru, D., Lemanceau, P., Griffiths, B., Hallin, S., Philippot, L., 2014. Recently identified microbial guild mediates soil N2O sink capacity. Nat. Clim. Chang. 4, 801–805.
Jørgensen, Nelson, 2004. Sulfide Oxidation in Marine Sediments: Geochemistry Meets Microbiology, 379. Geological Society of America, pp. 63–81.
Juhanson, J., Hallin, S., Söderström, M., Stenberg, M., Jones, C.M., 2017. Spatial and phyloecological analyses of nosZ genes underscore niche differentiation amongst terrestrial N2O reducing communities. Soil Biol. Biochem. 115, 82–91.
Kim, K.H., Heiss, J.W., Michael, H.A., Cai, W.-J., Laattoe, T., Post, V.E.A., Ullman, W.J., 2017. Spatial patterns of groundwater biogeochemical reactivity in an intertidal beach aquifer. J. Geophys. Res. Biogeosci. 122, 2548–2562.
Kim, K.H., Michael, H.A., Field, E.K., Ullman, W.J., 2019. Hydrologic shifts create complex transient distributions of particulate organic carbon and biogeochemical responses in beach aquifers. J. Geophys. Res. Biogeosci. 124, 3024–3038.
Körner, H., Zumft, W.G., 1989. Expression of denitrification enzymes in response to the dissolved oxygen level and respiratory substrate in continuous culture of Pseudomonas stutzeri. Appl. Environ. Microbiol. 55, 1670–1676.
Ligi, T., Truu, M., Oopkaup, K., Nõlvak, H., Mander, Ü., Mitsch, W.J., Truu, J., 2015. The genetic potential of N2 emission via denitrification and ANAMMOX from the soils and sediments of a created riverine treatment wetland complex. Ecol. Eng. 80, 181–190.
Lin, H., Dai, M., Kao, S.-J., Wang, L., Roberts, E., Yang, J.-Y.T., Huang, T., He, B., 2016. Spatiotemporal variability of nitrous oxide in a large eutrophic estuarine system: the Pearl River Estuary, China. Mar. Chem. 182, 14–24.
Lisa, J.A., Song, B., Tobias, C.R., Duernberger, K.A., 2014. Impacts of freshwater flushing on anammox community structure and activities in the New River Estuary, USA. Aquat. Microb. Ecol. 72, 17–31.
Liu, Q., Charette, M.A., Breier, C.F., Henderson, P.B., McCorkle, D.C., Martin, W., Dai, M., 2017. Carbonate system biogeochemistry in a subterranean estuary – Waquoit Bay, USA. Geochim. Cosmochim. Acta 203, 422–439.
Liu, X., Wu, J., Hong, Y., Jiao, L., Li, Y., Wang, L., Wang, Y., Chang, X., 2020. Nitrogen loss by nirS-type denitrifying bacterial communities in eutrophic coastal sediments. Int. Biodeterior. Biodegradation 150, 104955.
Lovley, D.R., Fraga, J.L., Coates, J.D., Blunt-Harris, E.L., 1999. Humics as an electron donor for anaerobic respiration. Environ. Microbiol. 1, 89–98.
Luijendijk, A., Hagenaars, G., Ranasinghe, R., Baart, F., Donchyts, G., Aarninkhof, S., 2018. The state of the world's beaches. Sci. Rep. 8, 6641.
Marchant, H.K., Holtappels, M., Lavik, G., Ahmerkamp, S., Winter, C., Kuypers, M.M.M., 2016. Coupled nitrification–denitrification leads to extensive N loss in subtidal permeable sediments. Limnol. Oceanogr. 61, 1033–1048.
Marchant, H.K., Tegetmeyer, H.E., Ahmerkamp, S., Holtappels, M., Lavik, G., Graf, J., Schreiber, F., Mussmann, M., Strous, M., Kuypers, M.M.M., 2018. Metabolic specialization of denitrifiers in permeable sediments controls N2O emissions. Environ. Microbiol. 20, 4486–4502.
O`Connor, A.E., Luek, J.L., McIntosh, H., Beck, A.J., 2015. Geochemistry of redox-sensitive trace elements in a shallow subterranean estuary. Mar. Chem. 172, 70–81.
O`Connor, A.E., Krask, J.L., Canuel, E.A., Beck, A.J., 2018. Seasonality of major redox constituents in a shallow subterranean estuary. Geochim. Cosmochim. Acta 224, 344–361.
Paranychianakis, N.V., Tsiknia, M., Kalogerakis, N., 2016. Pathways regulating the removal of nitrogen in planted and unplanted subsurface flow constructed wetlands. Water Res. 102, 321–329.
Rao, A.M.F., McCarthy, M.J., Gardner, W.S., Jahnke, R.A., 2008. Respiration and denitrification in permeable continental shelf deposits on the South Atlantic Bight: N2:Ar and isotope pairing measurements in sediment column experiments. Cont. Shelf Res. 28, 602–613.
Rotthauwe, J.H., Witzel, K.P., Liesack, W., 1997. The ammonia monooxygenase structural gene amoA as a functional marker: molecular fine-scale analysis of natural ammonia-oxidizing populations. Appl. Environ. Microbiol. 63, 4704–4712.
Roy, M., Martin, J.B., Cable, J.E., Smith, C.G., 2013. Variations of iron flux and organic carbon remineralization in a subterranean estuary caused by inter-annual variations in recharge. Geochim. Cosmochim. Acta 103, 301–315.
Saarenheimo, J., Rissanen, A.J., Arvola, L., Nykänen, H., Lehmann, M.F., Tiirola, M., 2015. Genetic and Environmental Controls on Nitrous Oxide Accumulation in Lakes. PLOS ONE 10 (3), e0121201.
Sáenz, J.P., Hopmans, E.C., Rogers, D., Henderson, P.B., Charette, M.A., Schouten, S., Casciotti, K.L., Sinninghe Damsté, J.S., Eglinton, T.I., 2012. Distribution of anaerobic ammonia-oxidizing bacteria in a subterranean estuary. Mar. Chem. 136–137, 7–13.
Santoro, A.E., 2010. Microbial nitrogen cycling at the saltwater–freshwater interface. Hydrogeol. J. 18, 187–202.
Santos, I.R.S., Burnett, W.C., Chanton, J., Mwashote, B., Suryaputra, I.G.N.A., Dittmar, T., 2008. Nutrient biogeochemistry in a Gulf of Mexico subterranean estuary and groundwater-derived fluxes to the coastal ocean. Limnol. Oceanogr. 53, 705–718.
Schutte, C.A., Joye, S.B., Wilson, A.M., Evans, T., Moore, W.S., Casciotti, K., 2015. Intense nitrogen cycling in permeable intertidal sediment revealed by a nitrous oxide hot spot. Glob. Biogeochem. Cycles 29, 1584–1598.
Schutte, C.A., Wilson, A.M., Evans, T., Moore, W.S., Joye, S.B., 2018. Deep oxygen penetration drives nitrification in intertidal beach sands. Limnol. Oceanogr. 63, S193–S208.
Seitzinger, S.P., Harrison, J.A., Dumont, E., Beusen, A.H.W., Bouwman, A.F., 2005. Sources and delivery of carbon, nitrogen, and phosphorus to the coastal zone: an overview of Global Nutrient Export from Watersheds (NEWS) models and their application. Glob. Biogeochem. Cycles 19, GB4S01.
Senga, Y., Mochida, K., Fukumori, R., Okamoto, N., Seike, Y., 2006. N2O accumulation in estuarine and coastal sediments: the influence of H2S on dissimilatory nitrate reduction. Estuar. Coast. Shelf Sci. 67, 231–238.
Shen, L.-d., Cheng, H.-x., Liu, X., Li, J.-h., Liu, Y., 2017. Potential role of anammox in nitrogen removal in a freshwater reservoir, Jiulonghu Reservoir (China). Environ. Sci. Pollut. Res. 24, 3890–3899.
Slomp, C.P., Van Cappellen, P., 2004. Nutrient inputs to the coastal ocean through submarine groundwater discharge: controls and potential impact. J. Hydrol. 295, 64–86.
Smith, R.L., Böhlke, J.K., Song, B., Tobias, C.R., 2015. Role of anaerobic ammonium oxidation (anammox) in nitrogen removal from a freshwater aquifer. Environ. Sci. Technol. 49, 12169–12177.
Song, B., Tobias, C.R., 2011. Chapter three - molecular and stable isotope methods to detect and measure anaerobic ammonium oxidation (anammox) in aquatic ecosystems. In: Klotz, M.G., Stein, L.Y. (Eds.), Methods in Enzymology. Academic Press, pp. 63–89.
Throbäck, I.N., Enwall, K., Jarvis, Å., Hallin, S., 2004. Reassessing PCR primers targeting nirS, nirK and nosZ genes for community surveys of denitrifying bacteria with DGGE. FEMS Microbiol. Ecol. 49, 401–417.
Valenzuela, E.I., Padilla-Loma, C., Gómez-Hernández, N., López-Lozano, N.E., Casas-Flores, S., Cervantes, F.J., 2020. Humic substances mediate anaerobic methane oxidation linked to nitrous oxide reduction in wetland sediments. Front. Microbiol. 11, 587.
Voss, M., Bange, H.W., Dippner, J.W., Middelburg, J.J., Montoya, J.P., Ward, B., 2013. The marine nitrogen cycle: recent discoveries, uncertainties and the potential relevance of climate change. Philos. Trans. R. Soc. B Biol. Sci. 368, 20130121.
Wang, Hong, Y., Wu, J., Xu, X.R., Bin, L., Pan, Y., Guan, F., Wen, J., 2015. Comparative analysis of two 16S rRNA gene-based PCR primer sets provides insight into the diversity distribution patterns of anammox bacteria in different environments. Appl. Microbiol. Biotechnol. 99, 8163–8176.
Ward, B.B., 2013. How nitrogen is lost. Science 341, 352–353.
Wittorf, L., Bonilla-Rosso, G., Jones, C.M., Bäckman, O., Hulth, S., Hallin, S., 2016. Habitat partitioning of marine benthic denitrifier communities in response to oxygen availability. Environ. Microbiol. Rep. 8, 486–492.
Wu, J., Hong, Y., Guan, F., Wang, Y., Tan, Y., Yue, W., Wu, M., Bin, L., Wang, J., Wen, J., 2016. A rapid and high-throughput microplate spectrophotometric method for field measurement of nitrate in seawater and freshwater. Sci. Rep. 6, 20165.
Wu, J., Hong, Y., He, X., Jiao, L., Wen, X., Chen, S., Chen, G., Li, Y., Huang, T., Hu, Y., Liu, X., 2018. Anaerobic ammonium oxidation in acidic red soils. Front. Microbiol. 9, 2142.
Wu, J., Hong, Y., Chang, X., Jiao, L., Li, Y., Liu, X., Xie, H., Gu, JD., 2019a. Unexpectedly high diversity of anammox bacteria detected in deep-sea surface sediments of the South China Sea. FEMS Microbiol. Ecol. 1 95 (3), fiz013.
Wu, J., Hong, Y., Ye, J., Li, Y., Liu, X., Jiao, L., Li, T., Li, Y., Bin, L., Wang, Y., 2019b. Diversity of anammox bacteria and contribution to the nitrogen loss in surface sediment. Int. Biodeterior. Biodegradation 142, 227–234.
Wu, J., Hong, Y., Wen, X., Li, Y., Wang, Y., Chang, X., 2020. Activity, abundance, and community composition of anaerobic ammonia–oxidizing (anammox) bacteria in sediment cores of the Pearl River Estuary. Estuar. Coasts 43, 73–85.

Xiao, K., Wu, J., Li, H., Hong, Y., Wilson, A.M., Jiao, J.J., Shananan, M., 2018. Nitrogen fate in a subtropical mangrove swamp: potential association with seawater-groundwater exchange. Sci. Total Environ. 635, 586–597.

Xie, H., Hong, Y., Liu, H., Jiao, L., Wu, J., Wang, L., 2020. Spatio-temporal shifts in community structure and activity of nirS-type denitrifiers in the sediment cores of Pearl River Estuary. PLoS One 15, e0231271.

Yoon, S., Nissen, S., Park, D., Sanford, R.A., Löffler, F.E., 2016. Nitrous oxide reduction kinetics distinguish bacteria harboring clade I NosZ from those harboring clade II NosZ. Appl. Environ. Microbiol. 82, 3793–3800.

Zannoni, D., 2004. Respiration in Archaea and Bacteria: Diversity of Prokaryotic Respiratory Systems. Springer.

Zhao, S., Zhou, J., Yuan, D., Wang, W., Zhou, L., Pi, Y., Zhu, G., 2020. NirS-type N2O-producers and nosZ II-type N2O-reducers determine the N2O emission potential in farmland rhizosphere soils. J. Soils Sediments 20, 461–471.

Zheng, Y., Hou, L., Liu, M., Liu, Z., Li, X., Lin, X., Yin, G., Gao, J., Yu, C., Wang, R., Jiang, X., 2016a. Tidal pumping facilitates dissimilatory nitrate reduction in intertidal marshes. Sci. Rep. 6, 21338.

Zheng, Y., Jiang, X., Hou, L., Liu, M., Lin, X., Gao, J., Li, X., Yin, G., Yu, C., Wang, R., 2016b. Shifts in the community structure and activity of anaerobic ammonium oxidation bacteria along an estuarine salinity gradient. J. Geophys. Res. Biogeosci. 121, 1632–1645.

Zhu, G., Wang, S., Wang, W., Wang, Y., Zhou, L., Jiang, B., Op den Camp, H.J.M., Risgaard-Petersen, N., Schwark, L., Peng, Y., Hefting, M.M., Jetten, M.S.M., Yin, C., 2013. Hotspots of anaerobic ammonium oxidation at land–freshwater interfaces. Nat. Geosci. 6, 103–107.